Composites Part B 305 (2025) 112677

Contents lists available at ScienceDirect

Composites Part B

journal homepage: www.elsevier.com/locate/compositesb

Braid-trusion of hollow thermoplastic composites using an expanding mandrel approach

Maissaloun El-Jakl *, Louis Laberge Lebel

Advanced Composites and Fibers Structures Laboratory (ACFSlab), High Performance Polymer and Composite Systems (CREPEC), Polytechnique Montreal, 2500 ch Polytechnique, Montreal, Qc, H3T 1J4, Canada

ARTICLE INFO

Keywords:
Braid
Pultrusion
Thermoplastic composite
Hollow structure
DREF

ABSTRACT

Braid-trusion involves the combination of a braiding machine with a pultrusion line to continuously produce composite structures with a constant cross-section and angle-oriented fibres. During the braid-trusion process, braids are subjected to tension and compression, which leads to braid deformation and fibre orientation variations. Successful braid-trusion of tubular structures requires a braid design methodology that accounts for braid deformations during its passage in the pultrusion die. Here, we present a braid design methodology for square hollow pultruded beams reinforced by triaxial braids. It is proposed that the internal perimeter of the braid, constrained by the braiding and pultrusion mandrels, must expand during pultrusion to account for braid consolidation. Two braid designs are proposed. The first has a constant braiding and pultrusion mandrel perimeter. The second has a braiding mandrel perimeter that is 0.9 times that of the pultrusion mandrel, referred to as the expanding mandrel approach. The design demonstrated the effect of an expanding mandrel in reducing fibre waviness by achieving similar braiding yarn lengths. Glass fibre/polyethylene terephthalate composites were pultruded with the constant and expanding mandrels. The constant mandrel braid-trusion failed while the expanding mandrel succeeded.

1. Introduction

Hollow composite structures find extensive use across various industrial sectors, including aerospace, automotive, marine, sports, and others, primarily due to their lightweight nature and remarkable strength-to-weight ratio [1]. However, the production of these structures presents a unique manufacturing challenge, particularly regarding the internal surface support and consolidation of the hollow structure [2]. Typically, hollow composite structures are manufactured by using thermosetting prepreg tapes and an inflatable bladder moulding technique [3]. This process involves wrapping the material around an inflatable bladder. The assembled components are then placed within a mould to define the external shape of the hollow structure. By pressurising the bladder, the prepregs are consolidated outward, ensuring proper consolidation. After curing, the bladder pressure is released, the bladder is collapsed, and it is removed. This manufacturing process requires skilled labour and the use of elastomers as bladder materials, which generally have limited temperature tolerance [2]. Thus, a demand arises to develop an automated manufacturing process suitable for efficiently producing hollow composite products with excellent mechanical properties.

Pultrusion involves the continuous production of composite material structures with constant cross-sections [4]. This manufacturing process is highly automated and allows for the mass production of structures capable of reaching high fibre volume fractions. Pultruded profiles have shown their ability to fulfil cost, mechanical, physical, and environmental durability criteria while delivering outstanding performance [5]. In recent decades, profiles manufactured through the pultrusion process have garnered growing attention across various industries [5]. Thermoset composite pultrusion is well-established and widely utilised, unlike pultrusion with thermoplastic matrices. Yet thermoplastic composites offer more advantages, as they have higher toughness and damage tolerance, are recyclable and can be joined by welding [4]. In thermoplastic pultrusion, the challenge lies in impregnation due to the molten viscosity being several orders of magnitude higher than that of thermoset polymers, typically ranging from 500 to 5000 Pa s [6]. To address the challenge posed by the high viscosity of thermoplastics, multiple hybrid yarn technologies have been developed to be used as input materials in thermoplastic pultrusion [7]. These yarns entail blending the polymer with the reinforcement fibres. Thereby, the

* Corresponding author.
E-mail address: Maissaloun.el-jakl@polymtl.ca (M. El-Jakl).

https://doi.org/10.1016/j.compositesb.2025.112677
Received 2 May 2024; Received in revised form 24 May 2025; Accepted 1 June 2025
Available online 2 June 2025

distance for the polymers to flow and impregnate the reinforcement fibres is reduced. Examples of thermoplastic hybrid yarns input material are prepregs, towpregs, commingled, co-wound and DREF yarns. Unlike other input material, DREF yarns have not been widely employed in thermoplastic pultrusion. DREF yarns consist of a continuous fibre core onto which discontinuous polymer fibres are spun using the friction spinning process [8]. DREF yarns offer benefits such as superior polymer/fibre distribution and improved handling compared to other types of hybrid yarns. To the author's knowledge, DREF yarns were not used in a pultruded braid structure.

In a hybrid yarn input material thermoplastic pultrusion, input materials are wound onto bobbins and placed in a creel that controls the unwinding tension [9]. Subsequently, yarns are drawn through a preheater, heated die, and then a cooling system, using a puller. At the end of the manufacturing line, a saw is positioned to cut the finished composite products. The heated die is where melting and impregnation happen. At that stage, the material in the die is referred to as a pultrudate. In a recent development, a series of heated dies arranged sequentially with a decreasing final cross-section has been utilised to enhance the impregnation of thermoplastic composites. This process is called multi-die pultrusion [8–12].

Braid-trusion is a production method for composite materials, where a braiding machine is linked with a pultrusion die to produce structures with constant cross-sections and off-axis fibre orientation in a continuous manner [14]. Braiding is a textile process in which three or more yarns are interlaced to produce a constant structure [15]. This process has received considerable attention in composites manufacturing due to the braid's mechanical properties, including good fatigue and crush resistance [16]. Michaeli et al. [17] was one of the first to introduce braiding to thermoplastic pultrusion and produced polypropylene/glass and polyether-ether-ketone/carbon structures. It was later reported that the orientation of braided fibres changes between the before and after pultrusion state [12,13]. Few experimental studies have explored the manufacturing of hollow pultruded thermoplastic composites, primarily focusing on tube structures [18–21], with one study introducing a square configuration [21]. However, none of them appear to have utilised a braid design methodology. It is suspected that the braid designs for pultrusion in the studies above relied on a trial-and-error approach. One of the first publications to introduce braid design for the braid-trusion process was by Laberge Lebel and Nakai [14]. The design was based on the circumferential deformation of a solid triaxial braid during consolidation. It was demonstrated that when subjected to compression within the pultrusion die, the braid's thickness decreases, leading to a reduction in the amplitude of the braiding yarns' oscillation within the braid structure. These oscillations characterise the yarn crimp, which is the actual length of the yarn over the fabric's length along the yarn path [22]. It was found that the braid structure needed to expand in its circumferential direction to accommodate the reduction in yarn crimp during braid consolidation [14]. Ghaedesharaf et al. [23] introduced a finite element model (FEM) of the 3D geometry of biaxial braids during pultrusion. Unlike triaxial braids, biaxial braids can also deform along their length under tensile load, as there are no axial yarns running along the braid. Using their FEM approach, Ghaedsharaf et al. [23] successfully designed a biaxial braid that could be pultruded with prediction of the braid's elongation and final diameter. Both models suggested that the braid-trusion process must account for the lengthening of yarns due to a reduction in the yarn's crimp. However, the models presented are complex, involving substantial computational time, and have not been validated for tubular braids. Braid-trusion of hollow thermoplastic composites using hybrid yarns was not thoroughly explored. Furthermore, all consolidation methods for the aforementioned tubular braid-trusion studies employed a straight section mandrel. Although braid-trusion of a solid structure is a complex process, braid-trusion of hollow structures using simultaneous internal and external tooling presents an even more significant challenge. To the authors' understanding, no studies have developed hollow braid-trusion design methodology using the alternative approach of an expanding mandrel.

The objective of this study is to develop a simplified hollow braid design methodology incorporating an expanding mandrel. A simple braid geometrical model is first introduced. The braid-trusion design methodology is described. Then, the design method was applied for braid-trusion of a square tubing on a constant and expanding cross-section mandrel. Braid-trusion experiments were conducted according to the design, and the braid-truded tubes were characterised.

2. Braid geometrical model

Fig. 1 (a) shows the geometrical model of a tubular triaxial braid comprising 24 braiding yarns (BY) and 12 axial yarns (AY) laid onto a rectangular mandrel with rounded corners. The braid is modelled using a 3D Computer-Aided Design (CAD) software (CATIA V5R19). A first set of 12 BYs, in blue on Fig. 1, spirals in a clockwise direction (CBY). The second set of 12 BYs, in green on Fig. 1 spirals in a counterclockwise direction (CCBY). The braid pitch (p) represents the distance for one BY to complete one full rotation around the braid axis. The braiding machine controls the pitch, that is, by the ratio of the pulling speed of the braid to the rotation speed of the braiding yarn carriers around the braider head [14]. Braids are commonly described with their braid angle (α). The braid angle depends on the braid's perimeter (C) and p, as,

$$\tan \alpha = C/p \tag{1}$$

Therefore, the higher the C/p ratio is, the higher the braid angle will be. Braids are typically made with angles α between 10° and 80° [24]. The BY path is modelled as a spline having definition points equally spaced onto a one-turn spiral (*i.e.*, for one pitch) around the mandrel. The radial position of the definition points is determined based on the mandrel surface and the thickness of the yarns. Fig. 1 (b) presents the cross-section of the braid showing a representation of the yarns' path. The mandrel has a width ($W_{mandrel}$), a depth ($H_{mandrel}$) and rounded edges radius ($R_{mandrel}$). For this braid architecture of 24 BY and 12 AY, it can be seen on Fig. 1 that the CBY passes above all the corners' AY, whereas the CCBY pass under them. This means that if the AY yarns have all the same thickness, the length of the CBY (L_{CBY}) passing over the corners will be significantly longer than the length of the CCBY (L_{CCBY}) passing close to the mandrel's corner surfaces ($L_{CBY} > L_{CCBY}$). To avoid this difference in length, the braid was deliberately modelled with six large AY yarns, (i.e., the LAY), and six small AY yarns (the SAY) in alternating positions. While yarns are typically represented by an elliptical or lenticular cross-section in kinematic textile modelling [14], for CAD simplicity, it was decided to model yarns with circular cross-sections. The diameter of the modelled circular yarns is equal to the yarn's thickness in the structure. The BY's thickness is b_{BY}. The thickness of the LAY and SAY is b_{LAY} and b_{SAY}, respectively. The thickness of the braid (t_{braid})is the summation of two b_{BY} and one b_{LAY}. In a braid architecture, the yarn's path oscillation is characterised by the crimp ratio (R_c) as,

$$R_c = L/l \tag{2}$$

where L is the actual length of the fibre and l is the fabric length along the yarn path. In Fig. 1, l is depicted in light blue. L and l can be measured on the CAD model. As R_c increases, the waviness of the fibres increases, and the axial mechanical properties of the composite decrease [22].

3. Braid-trusion design methodology

Fig. 2 illustrates the braid on a mandrel before and after pultrusion. Both braids are created with the model introduced in Section 2. The mandrel has a length of three braid pitches. The first pitch has mandrel and braid dimensions before pultrusion, and the last pitch has mandrel and braid dimensions after pultrusion. The middle pitch section presents

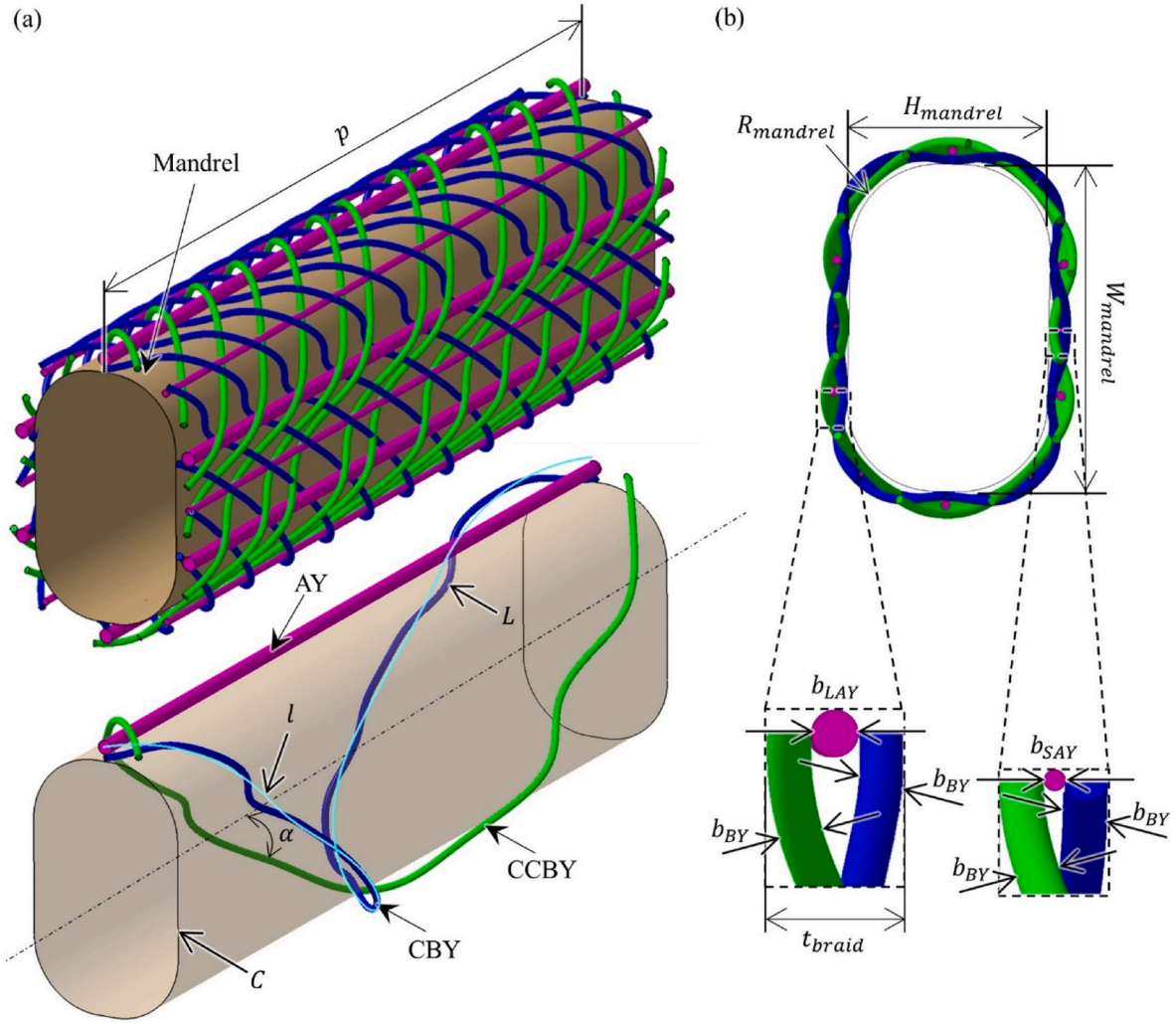

Fig. 1. (a) Tubular triaxial braid architecture on a rectangular mandrel presenting $\boldsymbol{p}$ and $\boldsymbol{\alpha}$. CBY and CCBY yarns are presented in blue and green, respectively. AY are presented in purple (b) Braid's cross-section showing a representation of the yarns' path. The enlarged view shows the yarns' diameter set to the yarns' thickness $\boldsymbol{b_{BY}}$, $\boldsymbol{b_{LAY}}$, and $\boldsymbol{b_{SAY}}$. (For interpretation of the references to colour in this figure legend, the reader is referred to the Web version of this article.)

the braid during the pultrusion process, which involves mandrel expansion within the dies. The before and after conditions and parameters of the braid will be referred to as in and out. One CBY and CCBY were isolated on top and bottom of Fig. 2 to showcase the length of the BY before ($L_{CBY,in}$, $L_{,CCBY,in}$) and after pultrusion ($L_{CBY,out}$, $L_{\ CCBY,out}$). The left-hand side of Fig. 2 shows view of the width of the mandrel before pultrusion (W_{in}) illustrating the CBY and CCBY braid angle before pultrusion ($\alpha_{CBY,in}$, $\alpha_{\ CCBY,in}$). The right-hand side shows view of the width of the mandrel after pultrusion (W_{out}) illustrating the braid angles after pultrusion ($\alpha_{CBY,out}$, $\alpha_{\ CCBY,out}$). The mandrel perimeters before (C_{in}) and after (C_{out}) pultrusion are shown. While the mandrel dimensions after pultrusion are selected according to the product's requirements, the dimensions of the mandrel before pultrusion (*i.e.,* the braiding mandrel's dimensions) can be proportionally reduced by a reduction ratio (R_m) defined as,

$$R_m = \frac{C_{in}}{C_{out}} \tag{3}$$

Since reinforcement yarns of glass or carbon fibres are inextensible, the braid perimeter must be expanded to account for the reduction of the crimp during consolidation in the pultrusion die. In other words, the braiding mandrel must be smaller than the pultrusion mandrel. The R_m can be selected using the CAD model of Fig. 2. The selection of the proper R_m for achieving a successful braid-trusion of hollow structure, it is determined by having the modelled length of the yarns before ($L_{CBY,in}$, $L_{CCBY,in}$) and after pultrusion ($L_{CBY,out}$, $L_{CCBY,out}$) equal. In case that $L_{CBY,in} > L_{CBY,out}$ or $L_{CCBY,in} > L_{CCBY,out}$, the yarns in the braid before pultrusion are longer than the available space in the braided structure. The extra yarn length will then wrinkle, leading to fibre waviness, which could be detrimental to the mechanical properties. Over time, the extra yarn length would accumulate at the pultrusion die entrance and could lead to blockage, stopping the pultrusion process. The alternative case that $L_{CBY,in} < L_{CBY,out}$ or $L_{CCBY,in} < L_{CCBY,out}$, the BY will apply a wrapping force on the pultrusion mandrel, causing high friction, which also leads to a stop in the pultrusion process, as the BY cannot elongate.

Fig. 3 shows a flow chart outlining the braid-trusion design methodology. The design methodology focuses initially on generating the CAD of the braid after pultrusion. The methodology has several inputs, some of which can be modified during the design, while others are fixed. The fixed set of inputs includes, firstly, the braid structure, which is determined by the braiding machine configuration. Secondly, the braid's internal geometry after pultrusion and thickness (t_{out}) are determined by the braid-trusion die and mandrel geometries and dimensions. The braid parameters are the set of inputs that can be modified during the design. This includes the braid pitch, which is initially defined to achieve the desired fibre angle for optimal product performance. The number of braid layers (N_{layer}) and the thicknesses of BY ($b_{BY,out}$) and LAY ($b_{LAY,out}$) are defined to satisfy Eq. (4). Unidirectional

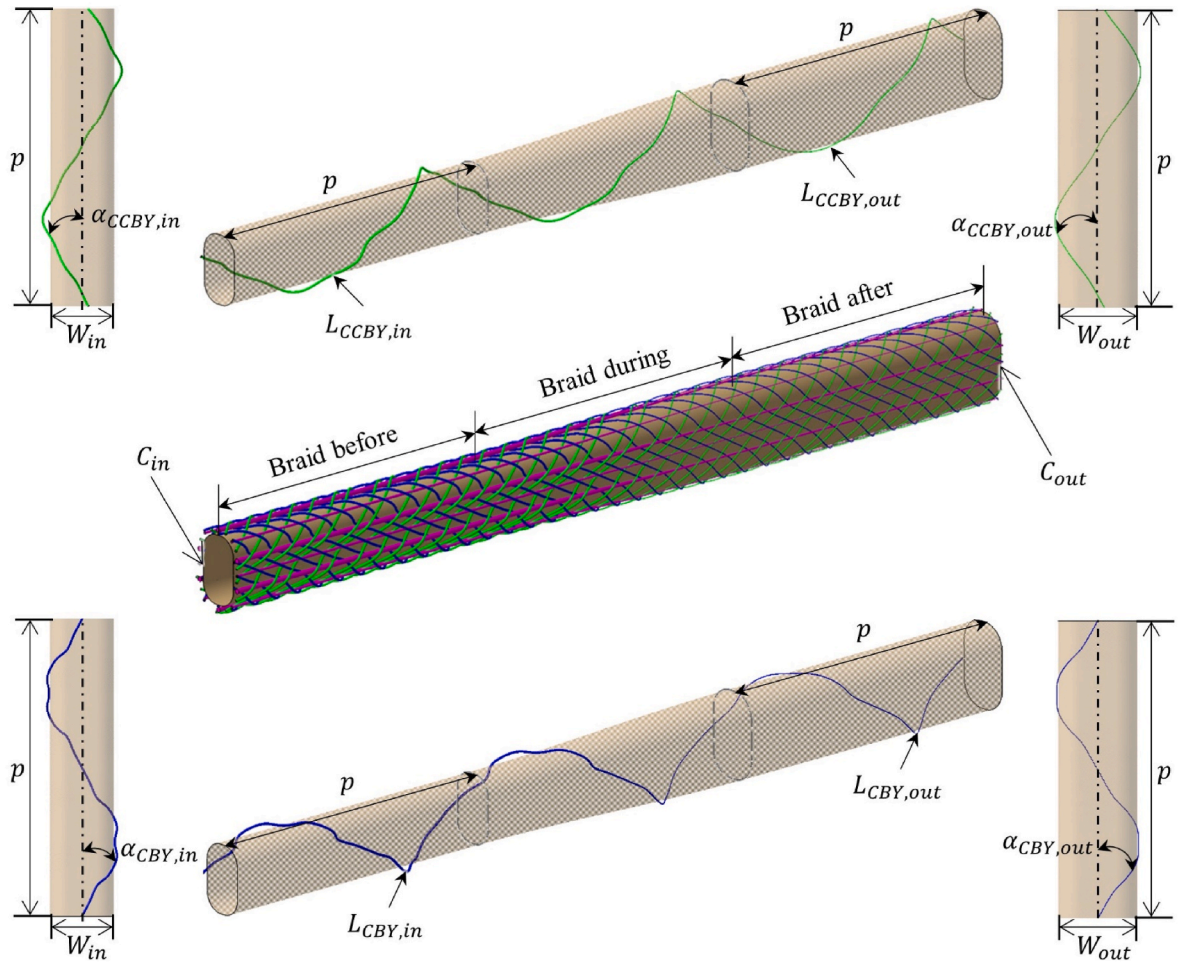

Fig. 2. Braid CAD presenting braid before, during and after pultrusion. On the top and bottom sections, one CBY and CCBY were isolated to showcase the length of the BY before and after pultrusion. On the left side, section cuts of $\boldsymbol{W_{in}}$ along $\boldsymbol{p}$ illustrate CBY and CCBY angles before pultrusion. On the right side, section cuts of $\boldsymbol{W_{out}}$ along $\boldsymbol{p}$ illustrate CBY and CCBY angles after pultrusion.

(UD) yarns can be added between braid layers. The thickness $b_{UD,out}$ can be defined to fill the vacant space between layers. Yarns are defined by their yarn count (i.e., the yarn's mass per unit length) and the material type density. At the starting point, all axial yarns are considered as LAY. The first step is to determine the yarn thickness of the model after pultrusion. The braid thickness after pultrusion, t_{out}, is known and expressed by,

$$t_{out} = N_{Layer}\left[2b_{BY,out} + b_{LAY,out}\right] \tag{4}$$

To solve Eq. (4), the ratio between $b_{BY,out}$ and $b_{LAY,out}$ is assumed to be the ratio of their yarn counts of the reinforcement ($F_{f,BY}$, $F_{f,LAY}$) and reinforcement material density ($\rho_{f,BY}$, $\rho_{f,LAY}$), such that,

$$\frac{b_{BY,out}}{b_{LAY,out}} = \frac{F_{f,BY} \times \rho_{f,LAY}}{\rho_{f,BY} \times F_{f,SAY}} \tag{5}$$

At this point, the braid after pultrusion can be modelled in the CAD software and the yarn lengths can be measured. The condition $L_{CBY} = L_{CCBY}$ is checked. If it is not verified, SAY are iteratively selected and strategically placed into the braid until the condition is verified. The $b_{SAY,\text{out}}$ is determined as a proportion of the $b_{LAY,\text{out}}$, analogous to Eq. (5) using,

$$b_{SAY,out} = \frac{F_{f,SAY} \times \rho_{f,LAY}}{\rho_{f,SAY} \times F_{f,LAY}} b_{LAY,out} \tag{6}$$

Where $F_{f,SAY}$ is the yarn count and $\rho_{f,SAY}$ is the density of the reinforcement of the SAY.

Once the braid after pultrusion is modelled, the fibre volume fraction (v_f) of the braid can be calculated using the area of reinforcement fibres (A_f) on the area of the pultruded product as,

$$v_f = \frac{A_f}{(A_{Die} - A_{mandrel})} \tag{7}$$

The A_f is calculated by,

$$A_f = \sum_{Layer\ 1}^{N} \left[N_{CBY} \frac{F_{f,CBY}}{\rho_{f,CBY}} \frac{L_{CBY,out}}{p} + N_{CCBY} \frac{F_{f,CCBY}}{\rho_{f,CCBY}} \frac{L_{CCBY,out}}{p} + N_{LAY} \frac{F_{f,LAY}}{\rho_{f,LAY}} + N_{SAY} \frac{F_{f,SAY}}{\rho_{f,SAY}} \right] + N_{UD} \frac{F_{f,UD}}{\rho_{f,UD}} \tag{8}$$

Eq. (8) is solved using the reinforcement yarn counts (F_f) , density (ρ_f) and quantity of yarns (N) for all yarn types (CBY, CCBY, LAY, SAY, and UD). Note that the yarns are assemblies of several DREF tows. The $L_{CBY,out}$ and $L_{CCBY,out}$ are measured on the CAD model.

The calculated v_f can be compared to a target value for the product. In case it is judged too far from the target value, the design of the braid after pultrusion can be adjusted by modifying any of the input braid parameters.

The next verification is the die filling condition. For successful pultrusion, it is recommended that the filling ratio (R_f) of the die be above 100 %. R_f is calculated according to,

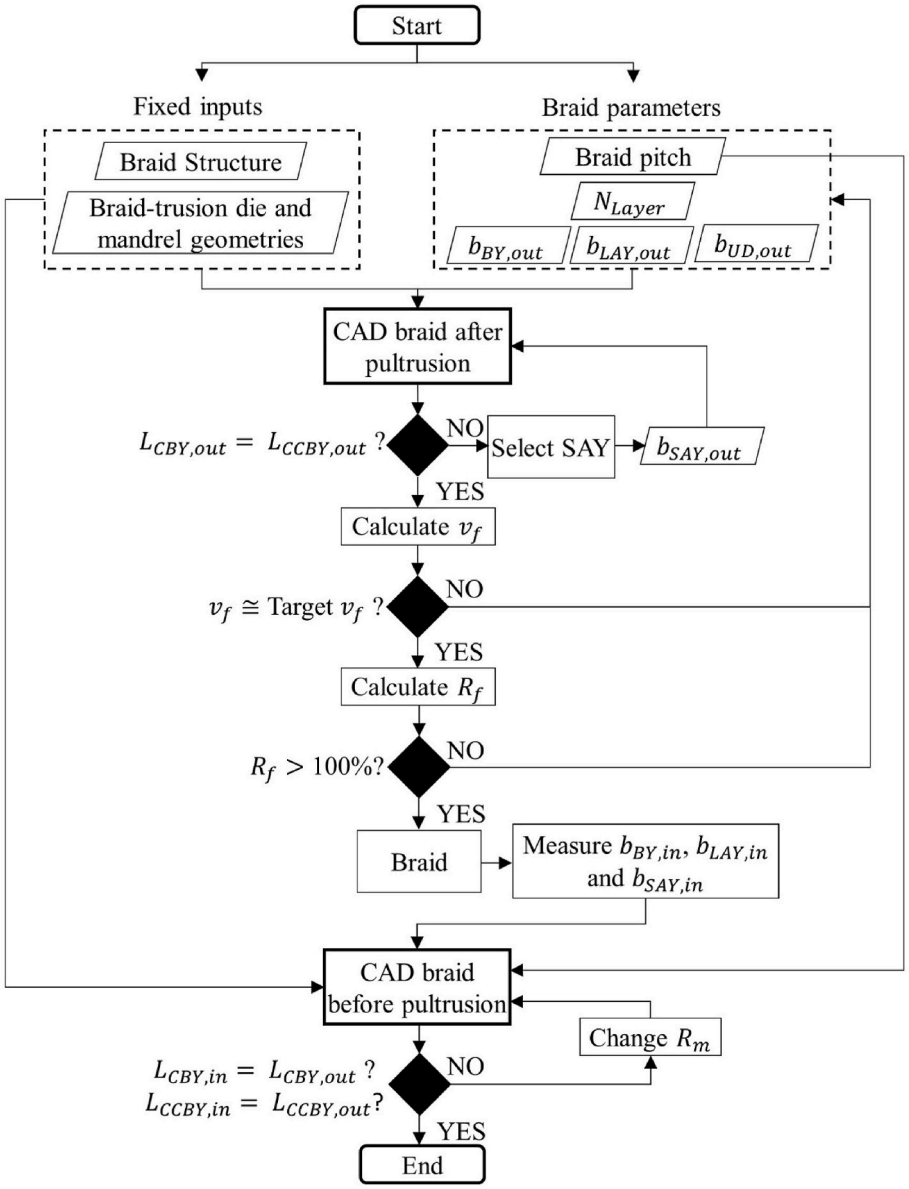

Fig. 3. Braid-trusion design methodology flow chart starting from the definition of the pultruded braid to get the braid parameters before pultrusion.

$$R_f = \frac{A_f + A_m}{(A_{Die} - A_{mandrel})} \tag{9}$$

In Eq. (9), A_m is the matrix area. This area is calculated using Eq. (8) with replacing the reinforcement yarn counts (F_f) and density (ρ_f) by the polymer's (F_m , ρ_m). If $R_f < 100$ %, input material composition should be changed to get a R_f superior to 100 %.

The braid-trusion design methodology then proceeds to the modelling of the braid before pultrusion. The important information needed are the yarn thicknesses. Since they are unconstrained, and without the use of advanced textile modelling methods, the yarn thickness must be measured in an actual braid. This braid must be formed onto a mandrel of the same dimensions as the pultrusion mandrel. The yarns' $b_{BY,\text{in}}$, $b_{LAY,\text{in}}$ and $b_{SAY,\text{in}}$ are measured. Once the braid before pultrusion is modelled, the $L_{CBY,in}$ and $L_{CCBY,in}$ are measured on the CAD. They are compared to the $L_{CBY,out}$ and $L_{CCBY,out}$. If they are not similar, R_m is then reduced iteratively until reaching $L_{CBY,in} = L_{CBY,out}$ and $L_{CCBY,in} = L_{CCBY,out}$.

4. Experimental

4.1. Materials

DREF yarns were used as the hybrid yarn input material for this study. The reinforcement fibre consisted of S2-glass fibres (GF) (SCG75, AGY) and the thermoplastic polymer was Polyethylene terephthalate fibres (PET) (staple fibre, Huvis Corporation). The DREF tows were obtained by friction spinning (Filspec Inc.). The DREF tow was composed of a GF core covered by discontinuous spun PET fibres. GF linear density (F_f) was 66 tex and PET linear density (F_m) was 38 tex. The DREF tow had a nominal volume fraction (($v_{n,f}$) of 50 %. A number of these small DREF tows were co-wound together in bobbins to form the larger yarns needed for the braid structure. Table 1 displays properties of the PET fibres used in DREF. The melting point (T_m), glass transition (T_g) and degradation temperatures were acquired using a Dynamic Scanning Calorimetry (MDSC 2000, TA instruments). Solid density was determined using a Pycnometer (Accupyc 1340, Micrometrics) and the melt density was measured by Pressure-Volume-Temperature analysis (pvT 100, ThermoHaake) at 270–285 °C. GF density was of 2.46 g/cm^3 as per

Table 1
Material properties.

Parameter	Unit	Value
Melting point	°C	257
Glass transition	°C	80
Degradation temperature	°C	295
Solid density	g/cm^3	1.43
Melt density	g/cm^3	1.06

AGY's technical datasheets.

4.2. Braid-trusion design application

The braid-trusion design mentioned above was used for a particular case. The fixed inputs are initially set as follows. A triaxial braid comprising 24 braiding yarns (BY) and 12 axial yarns (AY). This braiding machine arrangement produces a regular braid structure (2 over 2) [25]. Fig. 4 (a) and (b) presents the mandrel and die cross-section geometry. Both the mandrel and die had a rectangular cross-section with rounded corners. The mandrel depth, width and radius were 26,7 mm, 16.3 mm, and 7,25 mm. The mandrel perimeter was 84.3 mm. The die depth, width and radius were 29.7 mm, 19.3 mm, and 4.5 mm. With the mandrel inserted in the die, the pultruded profile wall thickness t_{out} = 1.5 mm and its area was $A_{Die} - A_{Mandrel} = 164mm^2$. The different radius values between the mandrel and the die creates a zone with increased thickness in each of the corners. Fig. 4 (c) shows the modelled braid structure after pultrusion. Two layers of braid were selected with four UD yarns added in the corners to fill the space created by the different mandrel and die radii. Two layers were chosen for the current study due to the fixed geometry and design requirements. It should be noted that increasing the number of layers would require adjusting the die entrance to accommodate the additional thickness. It may also impact the braiding process and the resulting composite properties.

Secondly, the braid-trusion design methodology was applied. The braid pitch was chosen at 105 mm for the first layer and 140 mm for the second layer. Table 2 shows the yarns selected for the braids. The BY and LAY were composed of 40 DREF tows. The UD were composed of 80

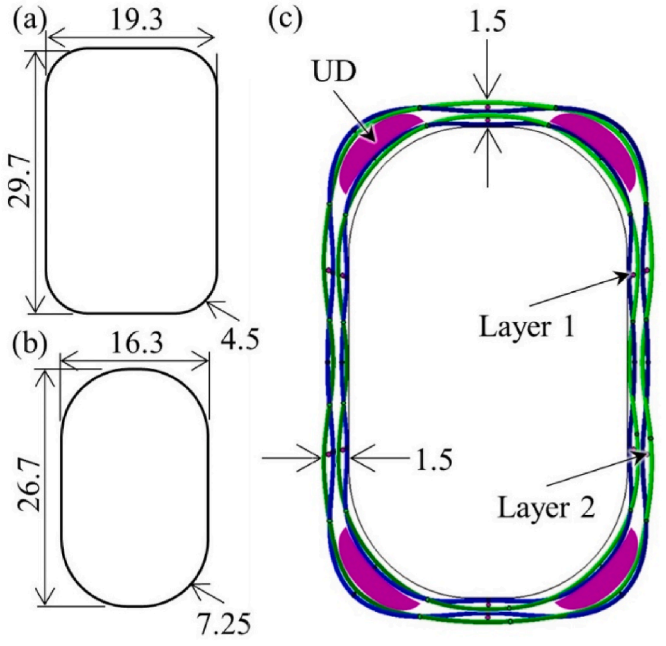

Fig. 4. (a) Die geometry, (b) mandrel geometry and (c) braid-truded structure after pultrusion showing its total thickness, two braid layers and 4 UD yarns at the corners. All dimensions are in mm.

Table 2
Parameters of the braid after and before pultrusion as determined by the braid-trusion methodology.

Yarns	DREF tow amount	ρ_f (g/cc)	ρ_m (g/cc)	F_f (tex)	F_m (tex)	b_{out} (mm)	b_{in} (mm)
BY	40	2.46	1.08	2640	1520	0.25	1.10
LAY	40	2.46	1.08	2640	1520	0.25	1.10
UD	80	2.46	1.08	5280	3040	0.5	n/a
SAY	8	2.46	1.08	528	304	0.05	0.22

DREF tows to fill the corners. The braid after pultrusion was then modelled with the verified condition of $L_{CBY,out} = L_{CCBY,out}$. To reach that condition, six LAY were replaced by six SAY containing 8 DREF tows. The v_f was calculated using Eqs. (7) and (8) and the parameters of Table 2 with $N_{CBY} = N_{CCBY} = 12$, $N_{LAY} = N_{SAY} = 6$ and $N_{UD} = 4$. The calculated v_f was 55 %, which corresponded to the target v_f. Following the design methodology, R_f was calculated and resulted in 128 %. To proceed with the braid methodology, a braid was made on a tube with a circumference in the same range as the pultrusion mandrel's perimeter. The tube had a diameter of 24 mm; its circumference was 75.3 mm. Subsequently, the yarn thicknesses in the braid were measured to be $b_{BY,in} = b_{LAY,in} = 1.1$ mm and $b_{SAY,in} = 0.22$ mm. The braid before pultrusion was then modelled.

Table 3 presents the modelled braids after and before pultrusion. There were two cases modelled. The first case modelled with a constant section mandrel ($R_m = 1$), while the second was modelled with an expanding cross-section mandrel ($R_m = 0.9$). The two layers' pitches are reported at 105 mm and 140 mm. After pultrusion, and for both cases, the first layer's mandrel perimeter was the mandrel tooling perimeter after pultrusion, that is 73.6 mm. The second layer internal perimeter was estimated to be a rounded rectangle with the dimensions calculated with,

$$W_{Layer2} = W_{Die} - 2\left(2b_{BY,out} + 2b_{LAY,out}\right) = 17.8, \quad (10)$$

$$H_{Layer2} = H_{Die} - 2\left(2b_{BY,out} + 2b_{LAY,out}\right) = 28.2, \quad (11)$$

$$R_{Layer2} = R_{Die} = 4.5\,. \quad (12)$$

The rationale for this estimation was to consider that the second layer's external surface matched the die's surface. The second layer internal perimeter was 84.3 mm. The $L_{CBY,out}$ and $L_{CCBY,out}$ are equivalent for each braided layers after pultrusion since these yarn lengths were adjusted by changing six LAY containing 40 DREF tows each by six SAY containing 8 DREF tows each in the braid modelling. Moreover, both $R_m = 1$ and $R_m = 0.9$ cases have identical yarn length for CBY and CCBY after pultrusion. This is because both cases' braids after pultrusion are modelled on the same mandrel. The last 3 columns of Table 3 present the modelled braids before pultrusion. The perimeters were calculated with mandrel dimensions modulated by the R_m factor. The $L_{CBY,in}$ and $L_{CCBY,in}$ are equivalent for each braided layer before pultrusion. This is expected since the braid structure after and before pultrusion is identical, and the yarn thicknesses are proportionally larger. For the two braided layers modelled for case $R_m = 1$, it is seen that the modelled yarn lengths before pultrusion are larger than the yarn lengths after pultrusion. The average difference between yarn lengths before and after pultrusion is 6.00 mm. Therefore, the extra yarn length in the braid before pultrusion will buckle in the pultrusion die and could result in detrimental fibre waviness. For the braid designed with $R_m = 0.9$, both layers show that $L_{CBY,CCBY,in}$ and $L_{CBY,CCBY,out}$ had an average difference of 1.25 mm. Therefore, braid-trusion on this expanding cross-section would exhibit less fibre waviness. The comparison of these two braid designs showed that applying the braid design methodology presented in Fig. 2 can result in a braid before pultrusion (i.e., at $R_m = 0.9$) that accounts for the reduction of the crimp during consolidation in the pultrusion die.

Table 3
Pitch, mandrel perimeters, measured length of CBY and CCBY after and before pultrusion, for the layers of braids with a constant section mandrel ($R_m = 1$) and an expanding cross-section mandrel ($R_m = 0.9$).

R_m (−)	Layer (−)	p (mm)	After Pultrusion			Before Pultrusion		
			C_{out} (mm)	$L_{CBY,out}$ (mm)	$L_{CCBY,out}$ (mm)	C_{in} (mm)	$L_{CBY,in}$ (mm)	$L_{CCBY,in}$ (mm)
1	1	110	73.6	131	131	73.6	137	138
	2	140	84.3	163	162	84.3	168	167
0.9	1	110	73.6	131	131	66.2	132	133
	2	140	84.3	163	162	75.9	164	163

4.3. Braiding

Two braids were manufactured following the braid design of Table 3. The braiding mandrels were circular tubing. For the case $R_m = 1$, the tubing diameter was 24 mm, and its circumference was 75.4 mm. The tubing circumference was approximately equal to the C_{in} of 73.6 mm of the modelled first layer braid. For the case $R_m = 0.9$, the tubing diameter was 22 mm, and its circumference was 69.1 mm. The tubing circumference was approximately equal to the C_{in} of 66.2 mm of the modelled first layer braid. The braiding machine (KBL-24-1-110, Xuzhou Henghui Braiding Machine Co., Ltd.) was set to braid with pitches of 105 mm for the first layer and 140 mm for the second layer. The carrier rotation speed was set to 0.06 RPS and the braid take-up speed was between 6.5 and 8.5 mm/s. The take-up speed was regulated to obtain the desired pitch length for each braid and layer. The tension in the carriers was around 3 N. The pitch length, carrier speed, and take-up speed are interdependent parameters in the braiding process. In this study, the desired pitch was predetermined based on the structural requirements of the braid. To achieve this target pitch, the carrier speed and take-up speed were adjusted accordingly. Tension settings were set to ensure fiber alignment without inducing yarn damage or excessive compaction. After braiding the first layer, the four UD were welded in their intended position over the SAY (See Fig. 4). The second layer was then over-braided on the first layer and UD assembly to obtain a braided preform. The braided preforms were approximately 2 m long. The braids' pitch and outside perimeter were measured.

4.4. Pultrusion apparatus and process

Fig. 5 (a) illustrates the pultrusion apparatus used for the pultrusion of the braided preforms. The braided preforms were removed from their mandrels and slid onto their respective pultrusion mandrels. The pultrusion mandrel was cantilevered from a fixed plate. The total mandrel length was 2 m. The preheating chamber was wrapped with a controlled heating tape set at 220 °C. To keep the mandrel centred in the die's cavities, rollers were positioned before the preheating chamber. Five heated pultrusion dies were used and set at 280 °C. The pultrusion dies were heated by cartridge heaters that were controlled using the feedback from type J thermocouples. Fans were installed to cool down the thin-walled tube of the last die to 160 °C. The braid was pulled through a puller system along the line at 25 mm/min. Fig. 5 (b) shows a cross-sectional view of the dies and mandrel with a constant cross-section. This mandrel was used for the pultrusion of the braided preform of case $R_m = 1$. Fig. 5 (c) shows a cross-sectional view of the dies and mandrel with an expanding cross-section. The mandrel's initial perimeter was 0.9 times its final one. This mandrel was used for the pultrusion of the braided preform of case $R_m = 0.9$ Fig. 5 (d) presents a cross-sectional view of one pultrusion die. All pultrusion dies had a 6° taper with a 17.4 mm length and an 8 mm straight section. The dies exit decreases gradually with an area decrease ratio of 4 %. The last die presented in Fig. 5 (e) had a 2° taper angle and a 1.6 mm thin-walled rectangular tube of 42.8 mm long.

4.5. Characterisation

Samples were taken from each braid-truded structure for the evaluation of both internal and external surfaces. The rectangular structures were cut with a precision saw, then polished with a 320-grit to improve the fibres' visibility. The images were analysed under a microscope (VHX 7000, Keyence). For each braid-truded structure, a sample was cut at the cross-section for impregnation assessment. The samples were embedded in epoxy resin (Epofix, Struers), then polished and analysed under a microscope using 200x magnification.

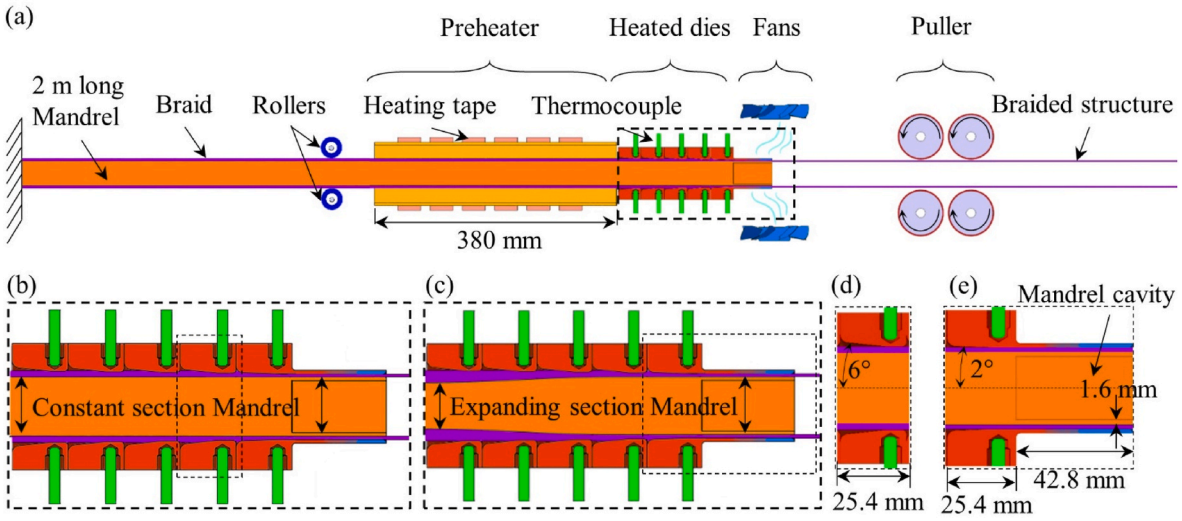

Fig. 5. (a) Pultrusion apparatus used for the discontinuous braid-trusion manufacturing. (b) Cross-sectional view of the dies and mandrel set up for the external consolidation only. (c) Cross-sectional view of the dies and mandrel set up for the internal consolidation. (d) Cross-sectional view of one pultrusion die. (e) Cross-sectional view of the cooling die.

5. Results and discussions

Table 4 presents the braid pitch (p) and outside braid perimeters (C) for both layers for cases $R_m = 1$ and $R_m = 0.9$. The average measured pitch of layer 1 indicated a difference of 5 mm with the braiding machine settings. The standard deviation on three measurements was above 5 mm. The average measured pitch of layer 2 matched the braiding machine settings of 140 mm. The braids outside perimeters of the first layers of each case do not match the modelled C_{in} of the second layer of each case as per Table 3. The outside perimeters of the first layers were 103 ± 7 mm for the case $R_m = 1$ and 98 ± 8 mm for the case $R_m = 0.9$. The modelled C_{in} for layer 2 per Table 3 were 84.3 mm and 75.9 mm, respectively. Moreover, the measured outside perimeters did not account for the UD welded on the first layer before overbraiding the second layer. The discrepancy is explained by the relatively simple modelling of the yarn and braids before pultrusion. This highlights the need for a more advanced modelling method for the braid before pultrusion.

Fig. 6 presents both braid-truded structures. Braid-truded structure $R_m = 1$ was pultruded with the constant section mandrel. Braid-truded structure $R_m = 0.9$ was pultruded with the expanding mandrel. Braid-trusion of 2 m long hollow thermoplastic composite structures using a multi-die pultrusion system was achieved. At the end of the pultrusion of case $R_m = 1$, the structure began to exhibit a stop-and-go motion due to slippage occurring between the braid-truded structure and the rollers of the puller. It was also observed that an accumulation of a larger diameter braid was at the die entrance. These observations support the braid-trusion design methodology introduced above. As shown in Table 3, for the braid designed with $R_m = 1$, the measured braiding yarn lengths on the CAD models were larger before than after pultrusion, such that $L_{CBY,in} > L_{CBY,out}$ and $L_{CCBY,in} > L_{CCBY,out}$. Moreover, the actual braid circumferences (See Table 4) were larger than the modelled ones (See Table 3) indicating an even larger actual $L_{CBY,in}$ and $L_{CCBY,in}$. The start-and-stop motion is attributed to the extra length of braided yarns that are compressed into the dies. The extra length probably created wrinkles and elevated friction resistance, as well as material accumulation at the die entrance. If the pultrusion with a constant section mandrel was continuous, the accumulation of braid at the entrance of the dies would have led to its interruption. On the other hand, the pultrusion for case $R_m = 0.9$ was done without stop-and-go, slippage in the puller, or interruptions.

Table 4
Pitch and perimeter measured on Braid 1 and Braid 0.9.

Case	Layer	p (mm)	C (mm)
$R_m = 1$	1	110 ± 7	103 ± 7
	2	140 ± 4	127 ± 7
$R_m = 0.9$	1	110 ± 5	98 ± 8
	2	140 ± 6	123 ± 7

The top two images of Fig. 7 shows the external (a) and internal (b) surfaces of the braid-truded structure for case $R_m = 1$. Fig. 7 (a) shows waviness and squashed fibres at the surface. The braid structure is barely recognisable. The braid pitch after pultrusion could not be measured. Waviness appeared less prominent on the internal surface shown in Fig. 7 (b). The internal surface's measured braid pitch was 154 ± 2 mm, which was 44 mm longer than thepitch of 110 ± 7 mm measured before pultrusion on layer 1 for case $R_m = 1$ (See Table 4). A longer pitch indicates that braiding yarns slid onto the axial yarns during the passage into the dies. It also explains the braid accumulation at the die entrance during pultrusion. These observations confirm that it is not recommended to use a constant mandrel size before and after pultrusion for braid-trusion of tubular structures using bulky hybrid yarns such as the GF/PET DREF yarns used in this study. The bottom two images of Fig. 7 shows the external (a) and internal (b) surfaces of the braid-truded structure for case $R_m = 0.9$. Both images show a braided structure that had a repeatable pattern and hardly any apparent fibre waviness. The measured pitches on the braid-truded structure for the case $R_m = 0.9$ were 143 ± 4 mm on the external surface and 119 ± 3 mm on the internal surface. When accounting for the standard deviations of the measured pitches before (See Table 4) and after pultrusion, it is most probable that the pitch did not change during pultrusion. These rather

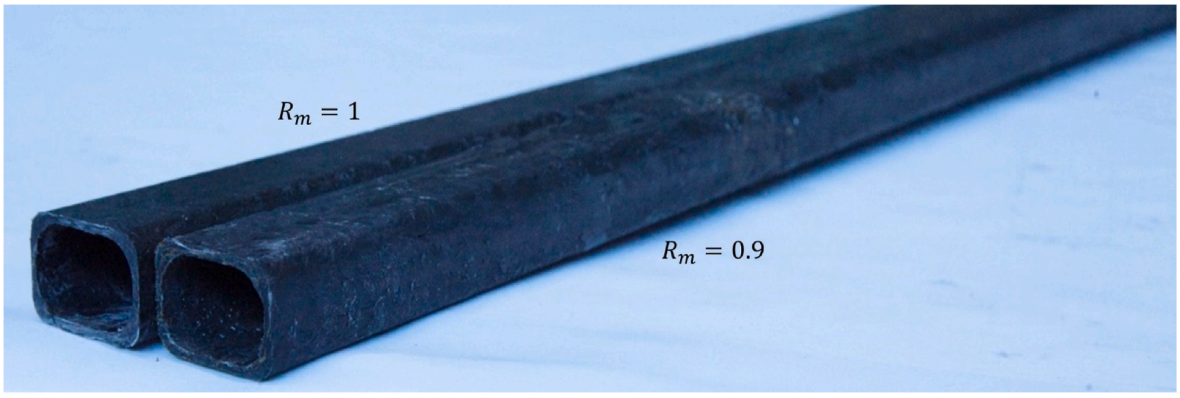

Fig. 6. Braid-truded structures for the cases $R_m = 1$ and $R_m = 0.9$.

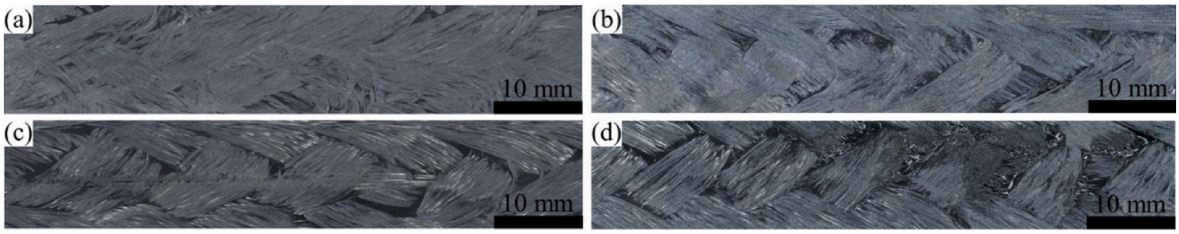

Fig. 7. Top: External (a) and internal (b) surfaces of the braid-truded structure for case $R_m = 1$. Bottom: External (c) and internal (d) surfaces of the braid-truded structure for case $R_m = 0.9$.

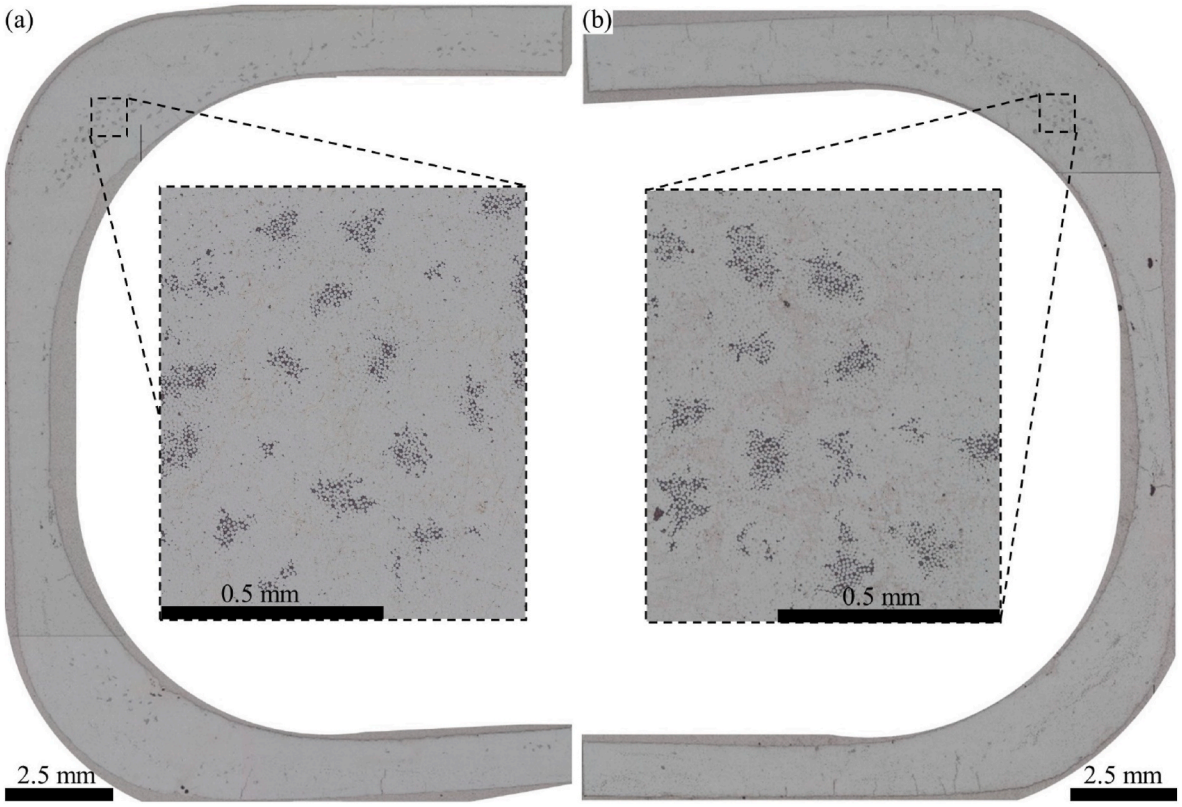

Fig. 8. Cross-sectional microscopic images of braid-truded 1 and 0.9 structures.

similar pitches before and after pultrusion indicated that the braided yarns did not slip onto the axial yarns during pultrusion. This is also supported by the fact that no braid accumulation and no stop-and-go motion were observed during pultrusion of the case $R_m = 0.9$. The fibre waviness reduction indicated on the braid-truded structure for case $R_m = 0.9$ compared to case $R_m = 1$ was attributed to the expanding mandrel. As the PET fibres melted in the DREF yarns, the GF loosened, and the expanding mandrel exerted tension on the GF present in the BY yarns. Based on the observations above, it can be supposed that the expanding mandrel approach in a braid-trusion of hollow thermoplastic composites effectively reduced fibre waviness (see Fig. 7).

Fig. 8 (a) and (b) displays the cross-sectional microscopic images of the braid-truded structure the cases $R_m = 1$ and $R_m = 0.9$, respectively. Black areas represent voids. In general, both structures presented a good impregnation quality. Enlarged images taken from the corners of both braid-truded structures showed unimpregnated fibre tows. These unimpregnated fibre tows are the ones that compose the UD yarns. The explanation for this difference in impregnation between UD yarns and braided ones may reside in the different axial (*i.e.*, along the pultrusion direction) and radial (*i.e.*, along the tow radius) permeabilities of both regions. More investigation should be done to explain the lower impregnation of the UD compared to the braided yarns.

6. Conclusion

This study proposes and demonstrates a braid-trusion design methodology for hollow structures. The methodology makes use of simple CAD models of the braid before and after pultrusion. To achieve a successful braid-trusion of tubular structures, it was suggested that the BY lengths before and after pultrusion needed to be equal. This braid design methodology shows that an expanding section mandrel ensures that the braid adjusts for its deformation while passing through the pultrusion dies. Braid-truded hollow thermoplastic composite structures using a multi-die pultrusion system were manufactured as an example. The absence of significant braid deformation at the die's entrance of the braid-truded structure with an expanding mandrel indicated that the braid design was adequate. However, to achieve better alignment between the design and experimental outcomes, a more advanced modelling method for the braid before pultrusion is required. Due to the lack of existing models on this subject, this model serves as an initial exploration, paving the way for future advancements. Subsequently, despite its simplicity, the model demonstrated promising results, suggesting that with refinement, continuous braid-trusion of hollow composites with an expanding mandrel could be feasible. Future studies will explore a broader range of reduction ratios, enabling a more comprehensive analysis of how different reduction ratios affect the performance of braided structures and further investigate the potential of the expanding mandrel approach. A precise fibre waviness assessment by CT scan will soon be conducted to measure the actual length of the BY yarns after pultrusion and compare it with the designed length. Nonetheless, the design procedure developed in this study could help with the production of high-performance braid-truded thermoplastic composites across various fields.

CRediT authorship contribution statement

Maissaloun El-Jakl: Writing – original draft, Validation, Methodology, Investigation, Conceptualization. **Louis Laberge Lebel:** Writing – review & editing, Supervision, Resources, Project administration, Funding acquisition, Conceptualization.

Declaration of competing interest

The authors declare that they have no known competing financial interests or personal relationships that could have appeared to influence the work reported in this paper.

Acknowledgements

The authors would like to acknowledge the financial support from the Natural Sciences and Engineering Research Council (NSERC, RDCPJ 543847-19) of Canada, PRIMA Quebec (R18-13-003), FilSpec Inc, Pultrusion Techniques, and Bauer Hockey ltd.

Data availability

Data will be made available on request.

References

[1] M. Naeimirad, R. Abuzade, V. Babaahmadi, R. E. Neisiany, R. Brull, F. Pursche, et « Hollow fiber reinforced polymer composites », dans Fiber Reinforced Composites, K. Joseph, K. Oksman, G. George, R. Wilson, et S. Appukuttan, Ed. Woodhead Publishing, 2021, p. 461-477.

[2] L. Lehnert, "Additive manufacturing of sacrificial cores for liquid moulding of composites", M.S. thesis, Department of Mechanical Engineering, McGill, Montreal, Canada, 2019.

[3] S.K. Bhudolia, G. Gohel, J. Kantipudi, K.F Leong, P. Gerard. Mechanical performance and damage mechanisms of thin rectangular carbon/Elium® tubular thermoplastic composites under flexure and low-velocity impact. Thin-Walled Struct 2021;165(April):107971.

[4] P.K. Mallick. Fibre-reinforced composites materials, manufacturing and design 2007;20(2).

[5] A. Vedernikov, A. Safonov, F. Tucci, P. Carlone. I. Akhatov, Pultruded materials and structures: a review. J Compos Mater 2020;54(26):4081–117.

[6] A. Safonov, P. Carlone, I. Akhatov. Mathematical simulation of pultrusion processes: a review. Compos Struct 2018;184(July 2017):153–77.

[7] K. Minchenkov, A. Vedernikov, A. Safonov, I. Akhatov. Thermoplastic pultrusion: a review. Polymers 2021;13(2).

[8] M.M.B. Hasan MMB, C. Cherif. Analysis of the influence of process parameters on the mechanical properties of carbon core friction spun hybrid yarns for composites. Fibres Text East Eur 2011;19:59-64.

[9] F. Lapointe, L. Laberge Lebel, Fiber damage and impregnation during multi-die vacuum assisted pultrusion of carbon/PEEK hybrid yarns, Polymer Compos 2019; 40 (S2):E1015-E1028.

[10] N. Alsinani, M. Ghaedsharaf. L. Laberge Lebel, Effect of cooling temperature on deconsolidation and pulling forces in a thermoplastic pultrusion process. Compos. Part B Eng. 2021;219(April):108889.

[11] F. Lapointe, A. Oswald, L. Laberge Lebel. Manufacturing of carbon/polyamide beam by vacuum assisted pultrusion. In *ECCM17-17th European confrence on composite materials*. 2016. p. 1–9.

[12] A. Oswald, F. Lapointe, L. Laberge Lebel, Multi-die, vacuum assisted pultrusion of flax/PLA thermoplastic biocomposite rods, In 17th European Conference on Composite Materials (ECCM 2016), Munich, Germany, 2016.

[13] M. Ghaedsharaf, J.E. Brunel, L. Laberge Lebel. Thermoplastic composite rod manufacturing using biaxial braid-trusion. In ECCM 2018 - 18th Eur. Conf. Compos. Mater. 2018.

[14] L. Laberge Lebel, A. Nakai. Design and manufacturing of an L-shaped thermoplastic composite beam by braid-trusion. Compos. Part A Appl Sci Manuf 2012;43(10): 1717–29.

[15] Y. Kyosev. Advances in braiding technology : specialized techniques and applications. Woodhead Publishing; 2016.

[16] M. Okano, A. Nakai, H. Hamada. Axial crushing performance of braided composite tubes. Int J Crashworthiness 2005;10(3):287–94.

[17] W. Michaeli, D. Jürss. Thermoplastic pull-braiding: pultrusion of profiles with braided fibre lay-up and thermoplastic matrix system (PP). Compos. Part A Appl Sci Manuf 1996;27(1):3–7.

[18] A. Memon, A. Nakai. Mechanical properties of jute spun Yarn/PLA tubular braided composite by pultrusion molding. Energy Proc 2013;34:818–829..

[19] A. Memon, A. Nakai. The processing design of jute spun yarn/PLA braided composite by pultrusion molding. Adv Mech Eng 2013;2013.

[20] T. Saito, A. Nakai, A. Ohtani. Effects of fabrication method of composite yarn intermediate material and resin melt viscosity on the impregnation properties and mechanical properties of PA66 fiber and glass fiber composites. J Thermoplast Compos Mater 2020;35(12)..

[21] J. Schäfer, T. Gries, R. Schuster, C. Lammel. Continious production of fibre reinforced thermoplastic composites by braiding pultrusion. ICCM Int. Conf. Compos. Mater. 2015;(July).

[22] Yang D. Investigation of braid geometry for complex braided composite structures. M.Phil. UK: Faculty of Science and Engineering,University of Mancheste; 2018.

[23] M. Ghaedsharaf, J.E. Brunel, L. Laberge Lebel. Multiscale numerical simulation of the forming process of biaxial braids during thermoplastic braid-trusion: predicting 3D and internal geometry and fiber orientation distribution. Compos. Part A Appl Sci Manuf 2021;150(July).

[24] Pastore C, Gowayed Y. Structure and mechanics of 2D and 3D textile composites. In: Schwartz P, editor. Structure and Mechanics of textile fibre assemblies. 2nd ed. Cambridge, UK: Woodhead Publishing; 2008. p. 145–90.

[25] A.A. Head, F.K. Ko, C.M. Pastore. Handbook of industrial braiding, Atkins and. Covington, KY: Pearce; 1989.